

# INSTA-BNN: Binary Neural Network with INSTA<sup>n</sup>ce-aware Threshold

Changhun Lee<sup>1</sup>, Hyungjun Kim<sup>1,3</sup>, Eunhyeok Park<sup>1</sup>, and Jae-Joon Kim<sup>2</sup>

<sup>1</sup> Pohang University of Science and Technology (POSTECH), Pohang, Korea  
 {changhun.lee, hyungjun.kim}@postech.ac.kr, canusglow@gmail.com

<sup>2</sup> Seoul National University, Seoul, Korea  
 kimjaeoon@snu.ac.kr

<sup>3</sup> SqueezeBits Inc., Seoul, Korea  
 hyungjun.kim@squeezebits.com

**Abstract.** Binary Neural Networks (BNNs) have emerged as a promising solution for reducing the memory footprint and compute costs of deep neural networks. BNNs, on the other hand, suffer from information loss because binary activations are limited to only two values, resulting in reduced accuracy. To improve the accuracy, previous studies have attempted to control the distribution of binary activation by manually shifting the threshold of the activation function or making the shift amount trainable. During the process, they usually depended on statistical information computed from a batch. We argue that using statistical data from a batch fails to capture the crucial information for each input instance in BNN computations, and the differences between statistical information computed from each instance need to be considered when determining the binary activation threshold of each instance. Based on the concept, we propose the Binary Neural Network with INSTA<sup>n</sup>ce-aware threshold (INSTA-BNN), which decides the activation threshold value considering the difference between statistical data computed from a batch and each instance. The proposed INSTA-BNN outperforms the baseline by 2.5% and 2.3% on the ImageNet classification task with comparable computing cost, achieving 68.0% and 71.7% top-1 accuracy on ResNet-18 and MobileNetV1 based models, respectively.

**Keywords:** Binary Neural Networks, activation threshold, activation distribution

## 1 Introduction

Deep neural networks (DNNs) are well-known for their abilities in image classification [8,15,27,28], object detection [16,17,25,26], and semantic segmentation [20,22] among other vision tasks. These DNNs usually achieve excellent accuracy by using a large model, but the massive model size also increases memory usage and computing cost. As a result, deploying these models on mobile devices frequently fail to meet the requirements for memory footprint or computing efficiency. To solve the issue, numerous network compression strategies

were introduced, including quantization, pruning, and efficient architecture design. Network binarization is one of the network quantization techniques in which weights and activations are quantized to 1-bit precision. Binary Neural Networks (BNNs) can therefore achieve  $32\times$  reduction in memory requirement compared to their 32-bit floating point counterpart model, and simple binary logic operations are much faster than 32-bit floating point operations.

However, BNNs usually suffer from accuracy degradation due to the aggressive data quantization. In spite of the great efficiency of BNN, the accuracy degradation limits the deployment of BNNs in real-world applications. Therefore, a large number of techniques have been introduced to minimize the accuracy degradation of BNNs focusing on weight binarization [23,24], shortcut connections [19], and threshold optimization [14,18,29].

In BNNs, only two values (+1 and  $-1$ ) are available for activations. As a result, the distribution of activations (or ratio of +1's to  $-1$ 's) plays a critical role in BNNs. Some of the previous works tried to train the thresholds of the binary activation function to control the activation distributions via back-propagation, commonly using batch-level statistical data to optimize thresholds [18,29]. As shown in Fig. 1, on the other hand, each instance in a batch has different statistical data in terms of mean, standard deviation, and skewness. Therefore, determining static thresholds using the batch-level statistical data alone may not provide the adequate threshold for each instance, thereby resulting in sub-optimal results in terms of overall accuracy.

In this work, we propose the INSTA-BNN of which the thresholds are calculated using the per-instance statistical information to consider the difference between the batch-wise and instance-wise characteristics. We found that calculating thresholds based on instance-wise statistical information (*e.g.* mean, variance, and skewness) significantly improves the accuracy of BNNs. Furthermore, we provide a method to combine the proposed instance-aware thresholds with the Squeeze-and-Excitation (SE) [9] technique so that one can choose to use a model with larger parameters when higher accuracy is needed. We assess the accuracy improvement and additional compute/parameter costs of the proposed schemes on the ImageNet classification dataset, and show that the proposed INSTA-BNN achieves higher accuracy with a similar number of parameters or operations.

Our contributions can be summarized as follows:

- We propose employing the instance-wise statistical information for determining the threshold of the binary activation for each instance.
- We propose combining the SE module into our proposed method. We also extend the idea of using instance-wise statistical information to the activation function for real-valued variables in BNNs.
- We apply the proposed schemes to various representative backbone models such as ResNet-18 and MobileNetV1 and demonstrate that the proposed BNNs outperform previous works by a significant margin.

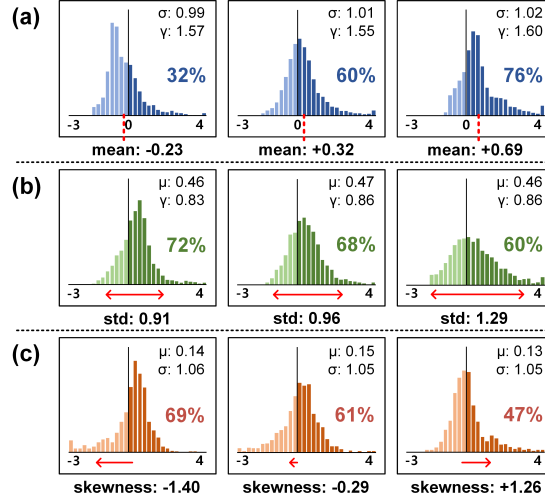


**Fig. 1.** Instance-wise (a) mean, (b) standard deviation, and (c) skewness of pre-activation from three different instances. The percentage in each distribution represents the ratio of +1’s in binary activation when sign function is used as activation function. When observing one component (e.g. mean ( $\mu$ ) for the (a) case), the other two (e.g. std ( $\sigma$ ), skewness ( $\gamma$ )) are matched to be as close as possible. The other two values are displayed on the top right of each subgraph.

## 2 Related works

### 2.1 Network Binarization

Network binarization can significantly reduce the size of a model and the compute cost by reducing the precision of weights and activations to 1-bit. Hubara *et al.* [10] proposed to binarize both the weights and activations of a model, and suggested to use the straight-through-estimator (STE) [1] to enable back-propagation through non-differentiable binarization function. XNOR-Net [24] introduced the real-valued scaling factor for binarized weights and activations to minimize the quantization error. To increase the representational capability of a model, an additional real-valued shortcut was suggested in Bi-real-net [19]. There are several more approaches to improve the accuracy of binarized networks, such as exploiting extra component [21,30], new model structures [3,19], and advanced training techniques [12,21,23]. In most previous BNNs, binarization of weights and activations were conducted with the Sign function:

$$x_b = \text{Sign}(x_r) = \begin{cases} +1, & \text{if } x_r \geq 0 \\ -1, & \text{if } x_r < 0 \end{cases} \quad (1)$$

In case of activations, Eq. (1) is also called the binary activation function. The  $x_r$  indicates a real-valued pre-activation value, and  $x_b$  is a binarized (+1 and -1) activation value. The value  $x_r$  is compared with the threshold of the binary activation function.

## 2.2 Threshold Optimization

Several works proposed to modify the thresholds of binary activation functions to improve the accuracy of BNNs. ReActNet [18] proposed the activation function with learnable threshold for which channel-wise parameters were trained via back-propagation. Although the proposed technique improved the accuracy of BNNs, the learned thresholds were fixed after training so that the same thresholds were always used for every input sample. Kim *et al.* [14] pointed out that back propagation alone cannot train the thresholds to have an optimal value. They demonstrated that the distribution of learned thresholds strongly depended on the initial values and did not deviate from the initial point much. While Kim *et al.* showed that initializing the thresholds with small positive values improved the accuracy of BNNs, they did not provide how to find optimal threshold values analytically. In summary, previous methods which tried to find optimal thresholds are sub-optimal, and all of them used the fixed threshold values during inference, failing to consider instance-wise statistical information of activation distributions.

## 3 Instance-Aware BNN

### 3.1 Importance of instance-wise statistical information

Compared to full precision DNNs, BNNs are more sensitive to the distribution of pre-activation values since activation output values are constrained to either +1 or -1. Batch Normalization (BN) [11] is usually used in BNNs because a small change in the distribution of pre-activation may cause a large difference in the distribution of the binary activation results. A BN layer normalizes the distribution of its input as well as stabilizes the training process of BNNs. Note that BN uses the statistical information of the entire training dataset to normalize the distribution. During training, a BN layer calculates the mean and variance of its input over the entire dataset. Once training is done, the BN layer uses the calculated mean and variance to normalize, scale, and shift its input.

In full precision DNNs, it may be sufficient to use statistical information of the entire dataset, but the distribution of each instance needs to be considered in BNNs due to the higher sensitivity to the distribution. Fig. 1a shows the distribution of pre-activations for three different images. Note that all three distributions are from the same layer and channel of a model, and they are the outputs of the normalization. It is clearly shown that the mean of each distribution has a non-zero value. This is because the mean value of each instance is different from the mean value of the entire dataset. The small difference in the pre-activation distribution results in the large difference in binary activation distribution. In Fig. 1a, the ratio of +1's in binary activations is shown for the cases when thresholds are fixed to 0. While the two distributions in the Fig. 1a (left and center) have the mean values that are relatively close to 0 (-0.23 and +0.32), the ratio of 1's shows a large difference (32% and 60%). To address the issue, we optimize the threshold values using per-instance statistical information.

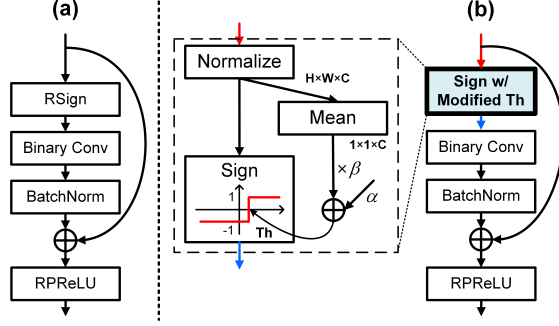


**Fig. 2.** Convolution blocks and the proposed module structure that uses the instance-wise mean information. (a) Binary convolution block structure without instance-aware modules. (b) Binary convolution block that contains the proposed module.

### 3.2 Instance mean-aware threshold

In this section, we introduce how to determine the instance-aware thresholds considering the instance-wise mean information. Fig. 2a shows the conventional block structure used in ReActNet [18]. To use the channel-wise learnable thresholds, ReActNet modified the Sign activation function as follows:

$$x_b = \begin{cases} +1, & \text{if } x_r \geq \alpha \\ -1, & \text{if } x_r < \alpha \end{cases} \quad (2)$$

Note that all the learnable variables used in this section are channel-wise variables. While the parameter  $\alpha$  was trained using back-propagation in ReActNet, we propose to replace it with an instance-aware threshold as follows:

$$x_b = \begin{cases} +1, & \text{if } x_r \geq TH \\ -1, & \text{if } x_r < TH \end{cases} \quad (3)$$

The instance-aware threshold ( $TH$ ) is calculated using per-instance statistical information. In this section, we first use the instance-wise mean information to calculate the  $TH$ . To calculate the difference between the per-instance mean and the mean over the entire dataset, we first normalize the pre-activation values using the BN layer without applying the affine transformation. After the normalization layer, the instance-wise mean is calculated as follows:

$$\tilde{x}_r = \frac{x_r - \hat{\mu}}{\hat{\sigma}} \quad E[\tilde{x}_r] = \frac{1}{H \times W} \sum_{i=1}^H \sum_{j=1}^W \tilde{x}_r(i, j), \quad (4)$$

where  $H$  and  $W$  are the height and width of the feature map. Using the instance-wise mean information, we formulate the instance-aware threshold as follows:

$$TH = \alpha + \beta E[\tilde{x}_r]. \quad (5)$$

The parameters  $\alpha$  and  $\beta$  are learned via back-propagation. In addition to the learnable parameter  $\alpha$  that is used in RSign of ReActNet, we use an additional scaling factor  $\beta$  which is related to instance-wise statistics. The proposed module is shown in Fig. 2b.

As shown in Fig. 1a, the instance-wise mean of pre-activation has a critical effect on the binary activation distribution. Therefore, using the instance-aware thresholds that adopt instance-wise mean information (Eq. (5)) can lead to better performance. We evaluate the effect of instance mean-aware thresholds on the ResNet-20 based model trained on the CIFAR-10 dataset. We compare the average accuracy of 6 runs with different random seeds. As shown in the top two rows in Fig. 3, the proposed instance mean-aware threshold improves the accuracy by 0.39% compared to the learnable threshold of RSign.

### 3.3 Addition of instance-wise variance and skewness

In previous section, we only considered instance-wise mean information to generate thresholds. However, variance and skewness of distribution also affect the binary activation distribution. In the Fig. 1b and c, distributions with different variance and skewness are shown. Even when the mean values are comparable, the characteristics of the binary activation distribution may vary depending on the variance or skewness. The skewness information, however, has not been considered in previous BNNs. To measure the skewness of a distribution, we used Fisher’s moment coefficient of skewness [31]:

$$\begin{aligned} Skewness(X) &= E\left[\left(\frac{X - \mu}{\sigma}\right)^3\right] = \frac{E[X^3] - 3\mu E[X^2] + 3\mu^2 E[X] - \mu^3}{\sigma^3} \\ &= \frac{E[X^3] - 3\mu\sigma^2 - \mu^3}{\sigma^3}. \end{aligned} \quad (6)$$

Similar to how we adopted the instance-wise mean information to determine thresholds in the previous section, we modify the instance-aware  $TH$  (Eq. (5)) to further consider variance and/or skewness of pre-activation.

We evaluate several options to add the influence of variance and skewness information on thresholds (Fig. 3). As expected, adding more statistical information for the instance-aware threshold improves the accuracy even further. When  $TH = \alpha + (\beta \times mean + \gamma \times skewness) \times var$ , we could achieve 87.32% accuracy which is about 0.9% higher than the baseline that uses ReActNet’s learnable threshold.

While using more per-instance statistical information improves accuracy, computing such statistical information for each instance requires high compute cost. For example, calculating skewness of pre-activation for each instance and each channel is costly. Here we introduce a simple alternative way to consider instance-wise mean, variance, and skewness at the same time. First, we can re-write the Eq. (6) as follows:

$$E[X^3] = (Skewness)\sigma^3 + 3\mu\sigma^2 + \mu^3. \quad (7)$$

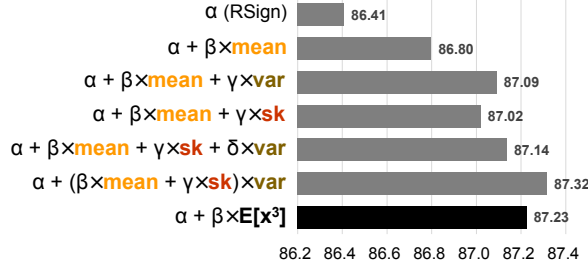


**Fig. 3.** Test accuracy of binary ResNet-20 based model on CIFAR-10 dataset when different instance-wise statistic information are used for thresholds. Various combinations of mean, variance (var), and skewness (sk) are evaluated.

We can see that the equation has information of mean, variance, and skewness and produces similar accuracy (87.23%) to the case that achieves the highest accuracy, 87.32% (Fig. 3). Therefore, we propose to use  $E[X^3]$  term instead of calculating all the mean, variance, and skewness of the pre-activation distribution separately. The proposed threshold can be expressed as:

$$TH = \alpha + \beta E[\tilde{x}_r^3] \quad x_b = \begin{cases} +1, & \text{if } \tilde{x}_r \geq TH \\ -1, & \text{if } \tilde{x}_r < TH \end{cases} \quad (8)$$

We name this threshold as **INSTAnce-aware Threshold (INSTA-Th)**. The INSTA-Th module is shown in Fig. 4a. Note that the Eq. (8) is identical to

$$TH' = -\alpha - \beta E[\tilde{x}_r^3] \quad x_b = \begin{cases} +1, & \text{if } \tilde{x}_r + TH' \geq 0 \\ -1, & \text{if } \tilde{x}_r + TH' < 0 \end{cases} \quad (9)$$

In our implementation, we used Eq. (9).

### 3.4 Squeeze-and-Excitation Module

Some of recent BNN works [21] used the Squeeze-and-Excitation (SE) module [9] to adopt a kind of instance-wise information. Although the SE module and INSTA-Th may look similar in that both of them use instance-wise information, there is a notable difference. The SE module was proposed to recalibrate inter-channel relationships while our INSTA-Th does not consider inter-channel relationships. As shown in Fig. 5, the SE module uses two fully-connected layers to assess the relative importance among different channels. On the other hand, the proposed INSTA-Th computes  $E[X^3]$  value channel-wise and then propagates the information to each channel independently. Note that the INSTA-TH focuses on the difference between batch-wise and instance-wise statistical information rather than the difference between channels.

Since the proposed INSTA-Th module and the SE module have different roles, we can use both schemes simultaneously to further improve the accuracy.

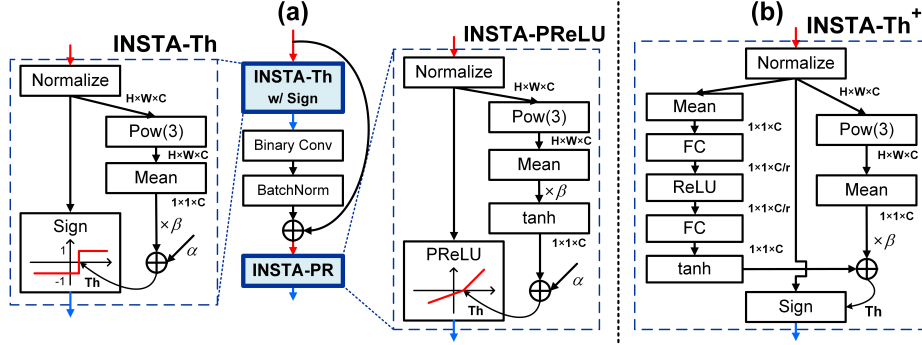


**Fig. 4.** Convolution blocks and the proposed module structures of INSTA-BNN. (a) Binary convolution Block that contains the proposed INSTA-Th and INSTA-PReLU modules. (b) INSTA-Th<sup>+</sup> module structure with SE-like block. INSTA-Th<sup>+</sup> can replace the INSTA-Th module in the structure of (a). Pow(3) indicates cubic operation,  $x^3$ .

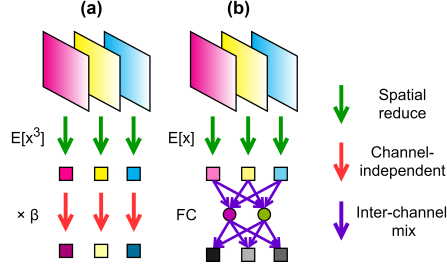


**Fig. 5.** Comparison of proposed INSTA-Th and SE module. (a)  $\beta E[\tilde{x}_r^3]$  component of INSTA-Th. (b) SE module. Non-linear functions are skipped for simplicity.

In Eq. (8), we modify the parameter  $\alpha$  to be the output of the SE-like module instead of the learnable parameter using back-propagation, as shown in Fig. 4b. We replace the Sigmoid function in the original SE module with  $\tanh$  function. To be more specific, we use the empirically found  $3 \cdot \tanh(x/3)$  to control the output range (Refer to Sec. 4.4 for more detail). In such a way, we intend  $\alpha$  to focus on channel-wise relationship and  $\beta E[X^3]$  to focus on instance-wise information. Note that  $\alpha$  is also an instance-aware variable in this case while it was a fixed value in previous works as in Eq. (2). We name the new threshold **INSTA-Th<sup>+</sup>**. While INSTA-Th<sup>+</sup> requires a larger number of parameters than INSTA-Th, it can be clearly seen that using both INSTA-Th and SE-like module improves the accuracy by a large margin (see Sec. 4.3). Therefore, we leave it as an option to select either INSTA-Th or INSTA-Th<sup>+</sup> depending on the requirement for the accuracy and parameter size.



### 3.5 Instance-aware PReLU

In recent works, additional activation functions such as ReLU and PReLU were used in BNNs for intermediate real-valued activations. ReActNet used additional learnable parameters for these PReLU layers (RPReLU) as well as the Sign layers (RSign) as shown in Fig. 2a. In addition to the INSTA-Th, we also propose replacing the learnable parameter (learnable shifts for x-axis) for RPReLU layers in ReActNet with instance-aware alternatives. We left the y-axis shift of RPReLU as it is. Fig. 4a shows the proposed **INSTAnce-aware PReLU (INSTA-PReLU)** which replaces the PReLU. In the INSTA-PReLU, we constrain the output range of  $\beta E[\tilde{x}^3]$ . In case of the INSTA-Th, the output range was not important since the end layer of INSTA-Th was the Sign function. However, as the PReLU layer does not constraint its output, extremely large values from the cubic operation may cause an unrecoverable problem in the network. As a result, we used the additional tanh function to constraint the output of the  $\beta E[\tilde{x}^3]$  term. The computation process of the modified PReLU layer is as follows:

$$\begin{aligned} \tilde{x} &= \frac{x - \hat{\mu}}{\hat{\sigma}} & TH_{PR} &= \alpha + \tanh(\beta E[\tilde{x}^3]) \\ y &= \begin{cases} \tilde{x} - TH_{PR}, & \text{if } \tilde{x} \geq TH_{PR} \\ \gamma(\tilde{x} - TH_{PR}), & \text{if } \tilde{x} < TH_{PR} \end{cases} \end{aligned} \quad (10)$$

Here,  $\gamma$  is a learnable slope parameter of the PReLU layer. We can further control the output range of  $\beta E[\tilde{x}^3]$  term by replacing the  $\tanh(x)$  function with the  $c \cdot \tanh(x/c)$ . We empirically found that  $c=3$  is worked well, so we chose to use  $3 \cdot \tanh(x/3)$  for all other experiments. The effect of INSTA-PReLU and different output range will be discussed in Sec. 4.4. Meanwhile, the parameter  $\alpha$  in INSTA-PReLU (Eq. (10)) can also be replaced by the SE-like module similar to the case in the previous section. We call the module as **INSTA-PReLU<sup>+</sup>**.

## 4 Experiments

In this section, we applied the proposed schemes to state-of-the-art BNN models and evaluated the accuracy improvement on ImageNet (ILSVRC12) dataset [6].

### 4.1 Experimental Setup

We used the PyTorch framework to implement state-of-the-art BNN models and the proposed INSTA-BNNs. We chose the ReActNet [18] as the baseline model. We replaced the RSign layer in ReActNet with INSTA-Th (or INSTA-Th<sup>+</sup>) module and the PReLU layer with INSTA-PReLU (or INSTA-PReLU<sup>+</sup>) module. The reduction ratio of 16 is used for INSTA-Th<sup>+</sup> and INSTA-PReLU<sup>+</sup>, if not specified. We followed the two-stage training strategy in [21] and used other detailed conditions in [18]. In the first stage, we trained a model with binary activation and full-precision weights from scratch. In the second stage,

we trained a BNN model by initializing it with pre-trained weights from the first stage. We followed the training recipe of [18] for both stages. We also applied the knowledge distillation using ResNet-34 as a teacher model. Note that our proposed INSTA-BNN does not rely on any specific BNN training methods, therefore all other options except module structure are kept the same as those of the baseline. To reduce the additional cost for computing the proposed scheme, we applied the 4-bit quantization to the activation just before the cubic operation and the 8-bit quantization to the weights of the SE-like module using a method from learned step size quantization (LSQ) [7]. Please refer to the Appendix B for more detail. For the ablation study, we used a simplified training process, in which we trained a BNN model directly from scratch for 90 epochs without help of the pre-trained or teacher models. Adam optimizer was used with an initial learning rate of 0.001, which is multiplied by 0.1 at epochs 40, 60, 80. Weight decay was not used, and learning rate warmup was used for the first 5 epochs. Precision other than 1-bit and 32-bit was not used for the ablation study.

## 4.2 Cost analysis

Here we introduce how we calculate the compute cost and parameter size of the proposed schemes. In INSTA-BNN, the additional operations are mainly from normalizing and cubic operations. The normalization process requires additional  $H \times W \times C$  floating point multiplications and the cubic operation requires  $3 \times H \times W \times C$  int4 multiplications. In terms of parameter size, each INSTA-Th and INSTA-PReLU requires four full-precision parameters per channel ( $\hat{\mu}$ ,  $\hat{\sigma}$ ,  $\alpha$ ,  $\beta$ ). INSTA-Th<sup>+</sup> and INSTA-PReLU<sup>+</sup> further require  $2C^2/r$  8-bit parameters for fully-connected layers of each SE-like module (r: reduction ratio). Note that while the compute cost of a SE-like module is usually considered to be negligible, its parameter size cannot be ignored in BNN models. We calculated total number of operations (OPs) as  $\text{OPs} = \text{FLOPs} + (\text{BOPs} / 64) + (\text{int4\_OPs} / 16)$ , following [18,19,32]. In case of parameters, binary weights are 1-bit, weights of SE-like modules are 8-bit, and other real-valued parameters and weights are considered as 32-bit. Other detailed rules are explained in the appendix.

## 4.3 Comparison on ImageNet Classification

In this section, we compare the accuracy and cost of previous BNN models and the proposed INSTA-BNN models. In Table 1, we grouped the models with similar model parameter sizes. For the proposed models, INSTA-BNN represents a model with INSTA-Th and INSTA-PReLU modules, and INSTA-BNN<sup>+</sup> represents a model with INSTA-Th<sup>+</sup> and INSTA-PReLU<sup>+</sup> modules. INSTA-BNN-ResNet18 / INSTA-BNN<sup>+</sup>-ResNet18 use the ReActNet-ResNet18 model as a backbone network while INSTA-BNN / INSTA-BNN<sup>+</sup> use the ReActNet-A model as a backbone network. However, for the experimental results, INSTA-BNN<sup>+</sup> (bottom row of Table 1) used the INSTA-Th<sup>+</sup> and INSTA-PReLU to keep the parameter cost in acceptable increments.

**Table 1.** Comparison of the number of operations, parameter size and ImageNet top-1 and top-5 validation accuracy of different BNN models. BOPs, int4\_OPs, and FLOPs mean the number of binary operations, int4 operations, and floating point operations, respectively. The values in parentheses of the 4th column indicate int4\_OPs. \* indicates that those numbers are from its original paper [2]. RN18 is an abbreviation for ResNet18.

Method	Bit width (W/A)	BOPS ( $\times 10^9$ )	FLOPS (int4_OPs) ( $\times 10^8$ )	OPs ( $\times 10^8$ )	Params (Mbit)	Top-1 Accuracy (%)	Top-5 Accuracy (%)
ResNet18 FP [5]	32/32	0	18.2	18.2	374	69.8	89.1
BNN [10]	1/1	1.70	1.20	1.47	28.1	42.2	67.1
XNOR-Net [24]	1/1	1.68	1.40	1.66	33.4	51.2	73.2
Bi-real Net 18 [19]	1/1	1.68	1.40	1.67	33.5	56.4	79.5
XNOR-Net++ [4]	1/1	1.68	1.42	1.68	33.5	57.1	79.9
IR-Net [23]	1/1	1.68	1.40	1.67	33.5	58.1	80.0
Bi-real Net 34 [19]	1/1	3.53	1.42	1.97	43.8	62.2	83.9
Real-to-Binary [21]	1/1	1.68	1.40	1.66	42.6	65.4	86.2
ReActNet-RN18 [18]	1/1	1.68	1.40	1.67	34.0	65.5	-
<b>INSTA-BNN-RN18</b>	1/1	1.68	1.44(0.10)	1.70	34.7	<b>67.3</b>	<b>87.4</b>
<b>INSTA-BNN<sup>+</sup>-RN18</b>	1/1	1.68	1.44(0.10)	1.71	37.4	<b>68.0</b>	<b>87.9</b>
ReActNet-A [18]	1/1	4.82	0.12	0.87	63.1	69.4	-
ReActNet-B [18]	1/1	4.69	0.44	1.17	68.0	70.1	-
<b>INSTA-BNN</b>	1/1	4.82	0.22(0.29)	0.99	65.1	<b>71.0</b>	<b>89.9</b>
High-Capacity Expert [2]	1/1	1.70*	1.10*	1.37	83.0	71.2	90.1
ReActNet-C [18]	1/1	4.69	1.40	2.14	84.7	71.4	-
<b>INSTA-BNN<sup>+</sup></b>	1/1	4.82	0.22(0.29)	0.99	71.0	<b>71.7</b>	<b>90.3</b>

Compared to BNN models with less than 50 Mbit parameters, the proposed INSTA-BNNs with ResNet-18 backbone achieved much higher accuracy. With a small overhead, INSTA-BNN with ResNet-18 backbone achieved 67.3% top-1 accuracy which is already 1.8% higher than ResNet-18 based ReActNet. In addition, with additional parameter cost, INSTA-BNN<sup>+</sup> with ResNet-18 backbone achieved even higher accuracy (68.0% top-1 accuracy) which is 2.5% higher than baseline, and only 1.8% lower than that of the full-precision ResNet-18 baseline. Similar improvement was achieved with larger BNN models. INSTA-BNN achieved 1.6% higher top-1 accuracy than ReActNet-A with marginal overhead. In case of INSTA-BNN<sup>+</sup>, it achieved higher top-1 accuracy than current state-of-the-art models, ReActNet-C and High-Capacity Expert [2], with much smaller parameter size and the compute cost.

The superiority of the proposed models is more clearly demonstrated in Fig. 6. The proposed INSTA-BNN models are placed in the upper-left side of previous state-of-the-art models in both accuracy vs. parameter size graph and accuracy vs. operations graph. Note that INSTA-BNN<sup>+</sup> models require more parameters than INSTA-BNN models, but additional OPs are negligible.

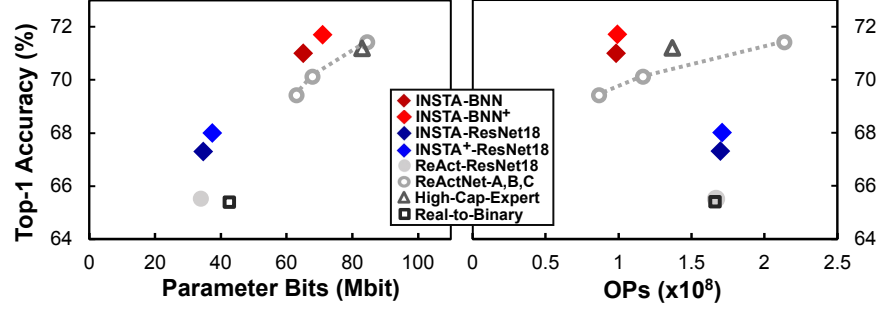


**Fig. 6.** (a) Parameter size versus ImageNet top-1 accuracy. (b) Number of operations (OPs) versus ImageNet top-1 accuracy.

#### 4.4 Ablation Study

**Effect of individual component in INSTA-BNN** Table 2 shows the effect of each component proposed in Sec. 3 on the ImageNet top-1 accuracy. Note that the absolute accuracy values are lower than those in Table 1 since the simplified training process (details in Sec. 4.1) was used for ablation study. First, using the instance-wise mean information on the threshold (Eq. (5)) improves the top-1 accuracy by 0.6% when compared to the baseline ReActNet model. On top of that, when variance and skewness information are added on the threshold (INSTA-Th), another 0.5% improvement is achieved. Replacing the learnable parameter  $\alpha$  in Eq. (8) with the SE-like module with reduction ratio of 8 achieves 61.7% top-1 accuracy that is 1.7% higher than baseline result. We also evaluate different combinations of INSTA-Th and INSTA-PReLU with and without the SE-like modules. When both modules use the SE-like module (INSTA-Th<sup>+</sup> and INSTA-PReLU<sup>+</sup>), we increase the reduction ratio to 16 to match the additional parameter cost. Regardless of where the SE-like module is applied, it improves the accuracy by large margin.

**Table 2.** The effect of each component of INSTA-BNN on the ImageNet top-1 accuracy. r indicates the reduction ratio of the fully-connected layers.

Network	Top-1 Acc. (%)
Baseline (RSign + RReLU)	60.0
Normalization and mean (Eq. (5))	60.6
INSTA-Th	61.1
INSTA-Th <sup>+</sup> (r=8)	61.7
INSTA-Th + INSTA-PReLU	62.1
INSTA-Th <sup>+</sup> + INSTA-PReLU (r=8)	63.0
INSTA-Th + INSTA-PReLU <sup>+</sup> (r=8)	62.8
INSTA-Th <sup>+</sup> + INSTA-PReLU <sup>+</sup> (r=16)	62.9

**Table 3.** The effect of the normalization layers. When normalization layers are removed from either INSTA-Th or INSTA-PReLU modules, the accuracy decreases.

Methods	Top-1 Acc. (%)
INSTA-Th	61.1
INSTA-Th <b>—norm</b>	60.8
INSTA-Th + INSTA-PReLU	62.1
INSTA-Th + (INSTA-PReLU <b>—norm</b> )	61.5

**Table 4.** ImageNet top-1 valid accuracy (%) according to the non-linear component of the each INSTA-PReLU and SE of INSTA-Th<sup>+</sup> module. Range means possible output range of each function.

	Range	INSTA-PReLU	SE (INSTA-Th <sup>+</sup> )
$\text{sigmoid}(x)$	0 $\sim$ 1	61.8	61.7
$\text{tanh}(x)$	-1 $\sim$ 1	61.9	61.4
$3\text{tanh}(x/3)$	-3 $\sim$ 3	<b>62.1</b>	<b>61.7</b>

**Effect of the normalization layer** In Sec. 3.2, we proposed using the normalization layer before calculating instance-wise mean information to capture the difference between instance-wise and batch-wise statistical data. Although the proposed modules can still make instance-aware thresholds without the normalization layer, we observed that removing the normalization from either INSTA-Th or INSTA-PReLU modules limits the performance of the modules (Table 3). When normalization layers are not used (—norm indication in the Table 3), the modules generate the threshold using the instance-wise statistical data themselves. In contrast, when the normalization layers are used, the difference between the instance-wise and batch-wise statistical data are used to generate the threshold, resulting in the higher accuracy.

**Effect of the threshold value range in INSTA-PReLU/INSTA-TH<sup>+</sup>** We use the bounded non-linear functions in the INSTA-PReLU, INSTA-Th<sup>+</sup>, and INSTA-PReLU<sup>+</sup> modules to map the threshold values in the constrained range (Fig. 4a, b). We evaluated three options;  $\text{sigmoid}(x)$ ,  $\text{tanh}(x)$ , and  $3*\text{tanh}(x/3)$ . Sigmoid is a widely used function and was used in the original SE work. However, the output of the sigmoid is always greater than zero, and hence it can only move the threshold to one direction from zero. On the other hand, tanh is bidirectional. We observed that the max value of  $\alpha$  in Eq. (8) for the trained networks was 2.45, so that we included  $3*\text{tanh}(x/3)$  in the options. From the Table 4,  $3*\text{tanh}(x/3)$  was found to be the best non-linear for the INSTA-PReLU, and it showed similar accuracy to that of sigmoid for SE module. Based on the results of Table 4 and the observed  $\alpha$  ranges, we used  $3*\text{tanh}(x/3)$  for the experiments in this paper.

## 5 Discussion: Reducing the inconsistent sign problem of binary convolution

CI-BCNN [30] discussed that one of the key reasons for the quantization errors in BNN is the sign mismatch between the binary convolution results and the

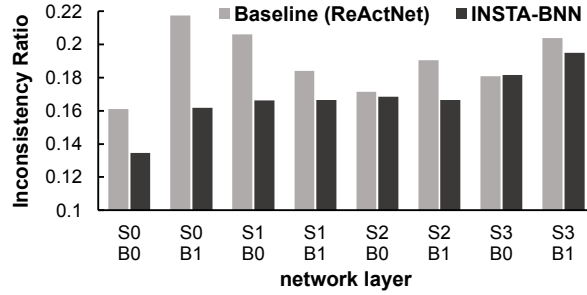


**Fig. 7.** Comparison of the inconsistent sign ratio between the baseline and the proposed INSTA-BNN. S and B represent the stage and the block of ResNet structure. Note that ResNet-18 consists of four stages with two blocks each, and therefore S0 B0 contains conv2 and conv3 layers.

counterpart full-precision results ( $\text{sign}(W_r \otimes A_r) \neq \text{sign}(W_b \oplus A_b)$ ). Then they tried to solve the inconsistency by imposing the channel-wise priors on the feature maps. Meanwhile, tuning the threshold is a direct way of changing the sign of binary activation, which consequently affects the sign of the binary convolution output. Hence, we checked the inconsistent ratio (ratio of pixels with inconsistent signs) for our baseline ReActNet and the proposed INSTA-BNN, and observed that the ratio was consistently lower in the INSTA-BNN (Fig. 7). We can see that our method is particularly effective in reducing the sign inconsistency of the earlier layers of the ResNet. The results demonstrate that our INSTA-BNN has the ability to reduce the quantization error by controlling the binary threshold without using channel-wise priors.

## 6 Conclusion

In this paper, we argue that the traditional way of deciding the threshold value of BNN activations using the batch-wise statistical information is sub-optimal. Instead, we demonstrate that the difference between the batch-wise information and the instance-wise information need to be considered to determine the better threshold values. Based on the idea, we propose the BNN with instance-aware threshold control (INSTA-Th), and demonstrate that the proposed BNN outperforms the previous BNNs by a large margin. We further improve the performance of the BNN with INSTA-Th by adding the instance-aware PReLU (INSTA-PReLU) and Squeeze-and-Excitation (SE) modules. Experimental results show that our INSTA-BNN<sup>+</sup> achieves the top-1 accuracy up to 71.7% on the ImageNet dataset.

## References

1. Bengio, Y., Léonard, N., Courville, A.: Estimating or propagating gradients through stochastic neurons for conditional computation. arXiv preprint arXiv:1308.3432 (2013)
2. Bulat, A., Martinez, B., Tzimiropoulos, G.: High-capacity expert binary networks. In: International Conference on Learning Representations (ICLR) (2021)
3. Bulat, A., Tzimiropoulos, G.: Binarized convolutional landmark localizers for human pose estimation and face alignment with limited resources. In: Proceedings of the IEEE International Conference on Computer Vision. pp. 3706–3714 (2017)
4. Bulat, A., Tzimiropoulos, G.: Xnor-net++: Improved binary neural networks. arXiv preprint arXiv:1909.13863 (2019)
5. Contributors, T.: Torchvision.models. <https://pytorch.org/vision/stable/models.html#classification> (2017), accessed: 2021-11-15
6. Deng, J., Dong, W., Socher, R., Li, L.J., Li, K., Fei-Fei, L.: Imagenet: A large-scale hierarchical image database. In: 2009 IEEE conference on computer vision and pattern recognition. pp. 248–255. Ieee (2009)
7. Esser, S.K., McKinstry, J.L., Bablani, D., Appuswamy, R., Modha, D.S.: Learned step size quantization. arXiv preprint arXiv:1902.08153 (2019)
8. He, K., Zhang, X., Ren, S., Sun, J.: Deep residual learning for image recognition. In: Proceedings of the IEEE conference on computer vision and pattern recognition. pp. 770–778 (2016)
9. Hu, J., Shen, L., Sun, G.: Squeeze-and-excitation networks. In: Proceedings of the IEEE conference on computer vision and pattern recognition. pp. 7132–7141 (2018)
10. Hubara, I., Courbariaux, M., Soudry, D., El-Yaniv, R., Bengio, Y.: Binarized neural networks. Advances in neural information processing systems **29** (2016)
11. Ioffe, S., Szegedy, C.: Batch normalization: Accelerating deep network training by reducing internal covariate shift. In: International conference on machine learning. pp. 448–456. PMLR (2015)
12. Kim, H., Kim, K., Kim, J., Kim, J.J.: Binaryduo: Reducing gradient mismatch in binary activation network by coupling binary activations. In: International Conference on Learning Representations (2019)
13. Kim, H., Kim, Y., Kim, J.J.: In-memory batch-normalization for resistive memory based binary neural network hardware. In: Proceedings of the 24th Asia and South Pacific Design Automation Conference. pp. 645–650 (2019)
14. Kim, H., Park, J., Lee, C., Kim, J.J.: Improving accuracy of binary neural networks using unbalanced activation distribution. In: Proceedings of the IEEE/CVF Conference on Computer Vision and Pattern Recognition. pp. 7862–7871 (2021)
15. Krizhevsky, A., Sutskever, I., Hinton, G.E.: Imagenet classification with deep convolutional neural networks. Advances in neural information processing systems **25**, 1097–1105 (2012)
16. Lin, T.Y., Goyal, P., Girshick, R., He, K., Dollár, P.: Focal loss for dense object detection. In: Proceedings of the IEEE international conference on computer vision. pp. 2980–2988 (2017)
17. Liu, W., Anguelov, D., Erhan, D., Szegedy, C., Reed, S., Fu, C.Y., Berg, A.C.: Ssd: Single shot multibox detector. In: European conference on computer vision. pp. 21–37. Springer (2016)
18. Liu, Z., Shen, Z., Savvides, M., Cheng, K.T.: Reactnet: Towards precise binary neural network with generalized activation functions. In: European Conference on Computer Vision. pp. 143–159. Springer (2020)

19. Liu, Z., Wu, B., Luo, W., Yang, X., Liu, W., Cheng, K.T.: Bi-real net: Enhancing the performance of 1-bit cnns with improved representational capability and advanced training algorithm. In: *Proceedings of the European conference on computer vision (ECCV)*. pp. 722–737 (2018)
20. Long, J., Shelhamer, E., Darrell, T.: Fully convolutional networks for semantic segmentation. In: *Proceedings of the IEEE conference on computer vision and pattern recognition*. pp. 3431–3440 (2015)
21. Martinez, B., Yang, J., Bulat, A., Tzimiropoulos, G.: Training binary neural networks with real-to-binary convolutions. In: *ICLR* (2020)
22. Noh, H., Hong, S., Han, B.: Learning deconvolution network for semantic segmentation. In: *Proceedings of the IEEE international conference on computer vision*. pp. 1520–1528 (2015)
23. Qin, H., Gong, R., Liu, X., Shen, M., Wei, Z., Yu, F., Song, J.: Forward and backward information retention for accurate binary neural networks. In: *Proceedings of the IEEE/CVF Conference on Computer Vision and Pattern Recognition*. pp. 2250–2259 (2020)
24. Rastegari, M., Ordonez, V., Redmon, J., Farhadi, A.: Xnor-net: Imagenet classification using binary convolutional neural networks. In: *European conference on computer vision*. pp. 525–542. Springer (2016)
25. Redmon, J., Divvala, S., Girshick, R., Farhadi, A.: You only look once: Unified, real-time object detection. In: *Proceedings of the IEEE conference on computer vision and pattern recognition*. pp. 779–788 (2016)
26. Ren, S., He, K., Girshick, R., Sun, J.: Faster r-cnn: Towards real-time object detection with region proposal networks. *Advances in neural information processing systems* **28**, 91–99 (2015)
27. Simonyan, K., Zisserman, A.: Very deep convolutional networks for large-scale image recognition. *arXiv preprint arXiv:1409.1556* (2014)
28. Szegedy, C., Liu, W., Jia, Y., Sermanet, P., Reed, S., Anguelov, D., Erhan, D., Vanhoucke, V., Rabinovich, A.: Going deeper with convolutions. In: *Proceedings of the IEEE conference on computer vision and pattern recognition*. pp. 1–9 (2015)
29. Wang, P., He, X., Li, G., Zhao, T., Cheng, J.: Sparsity-inducing binarized neural networks. In: *Proceedings of the AAAI Conference on Artificial Intelligence*. vol. 34, pp. 12192–12199 (2020)
30. Wang, Z., Lu, J., Tao, C., Zhou, J., Tian, Q.: Learning channel-wise interactions for binary convolutional neural networks. In: *Proceedings of the IEEE/CVF Conference on Computer Vision and Pattern Recognition*. pp. 568–577 (2019)
31. Wikipedia contributors: Skewness — Wikipedia, the free encyclopedia. <https://en.wikipedia.org/w/index.php?title=Skewness&oldid=1049351964> (2021), [Online; accessed 15-November-2021]
32. Zhang, Y., Zhang, Z., Lew, L.: Pokebnn: A binary pursuit of lightweight accuracy. *arXiv preprint arXiv:2112.00133* (2021)



## Appendix

### A Experimental setup for CIFAR-10 dataset

The extensive experiments in the main paper, Fig. 3, were conducted using ResNet-20 [8] with CIFAR-10 dataset. More precisely, we used ResNet-20 with additional skip connections from [19] and attached PReLU after the element-wise addition of residual path and identity shortcut. Therefore, the convolution block structure is similar to the block used in ReActNet [18] (Fig. 2a of the main paper). We used AdamW optimizer with a weight decay value of  $1e-4$ , and the networks were trained up to 400 epochs. The initial learning rate was 0.003, and the cosine annealing schedule was used. The batch size was set to 256. We used the weight scaling factor from [24].

### B Details and training methods for the quantization

As described in Sec. 4.1 of the main paper, we quantized the activation just before the cubic operation and the weights of the SE-like modules. We followed the fine-tuning scheme of LSQ [7]. We used layer-wise learnable step size for 4-bit activation quantization and channel-wise step size for 8-bit weight quantization. Symmetric quantization ( $Q_N = 2^{b-1}$  and  $Q_P = 2^{b-1} - 1$ , encoding with  $b$  bits) was applied for both.

After the two-stage training, we obtain the conventional BNN with binary convolution blocks and all other real-valued components. Then we fine-tuned the BNN model for 90 epochs to apply 4-bit quantization to the activation just before the cubic operation. The initial learning rate was 0.0001 and we used a linear learning rate decay scheduler. When the SE module is used, additional 5 epochs of fine-tuning were performed with 8-bit SE weights. We did not use the weight decay for either fine-tuning. The quantization resulted in negligible accuracy loss, and in some cases produced slightly better accuracy.

### C Detailed rules for the cost analysis

In this paper, we manually calculated the computation cost and parameter size of the previous methods and our proposed INSTA-BNN. In this section, we introduce additional detailed rules that we used to calculate the computation cost of the network. First, we only counted the number of floating point (FP) multiplication for the FLOPs calculation following the method used in [18,19]. That is, we count one floating point multiply-accumulate (MAC) as one FLOP, so our FLOPs calculation includes a pair of multiplication and addition. The same rule applies to the calculation of BOPs. In case of int4\_OPs, cubic operation has fewer additions than multiplications, so the calculated costs indicate the upper bound values.

For the Batch Normalization layer, we assumed that the layer has  $2 \times C$  sets of parameters because 4 BN parameters can be merged into the scale and shift

terms offline. FP multiplication cost of BN layer is  $H \times W \times C$ . However, when the Sign function directly comes after BN layer, FP multiplication cost is removed and we only need  $1 \times C$  set of parameters, following [13]. In case of using weight scaling factor [24], the element-wise FP multiplication cost of  $H_{out} \times W_{out} \times C_{out}$  is required, where the subscript *out* means the output of the convolution. However, when a method has conv-BN layer ordering, instead of doing element-wise multiplication for each scaling factor and BN layer, we can first multiply analytically calculated scaling factor and the merged BN scale parameter. In this way, we can also remove one set of  $H \times W \times C$  element-wise multiplications. We ignored the operation cost for PReLU layer because the cost may vary depending on the implementation, and its effect is very small compared to the real-valued convolution cost.

Finally, we assumed that all the ResNet-based methods use the shortcut option B reported in [8]. In addition, we assumed that average pooling, real-valued  $1 \times 1$  convolution, and BN layer are used for the downsampling path, except the BNN [10] case, which uses binary  $1 \times 1$  convolution.

Our proposed INSTA-Th needs  $4 \times C$  set of parameters. For INSTA-PReLU, total five parameters per channel (including the learned slope of PReLU) are required. Both module need  $H \times W \times C$  floating point operations for normalization and  $3 \times H \times W \times C$  4-bit operations for cubic operation. This is because when a cubic operation is considered as two element-wise multiplications, the intermediate result becomes 8-bit, and the multiplication of this result and another 4-bit operand can be calculated with two 4-bit multiplications. For INSTA-Th, Additional  $2 \times C$  operations are needed for spatial averaging and multiplying channel-wise parameters. We need extra  $3 \times C$  operations for INSTA-PReLU because we additionally use  $3 \times \tanh(x/3)$  for INSTA-PReLU.

We also considered the additional cost caused by the quantization. Due to the channel-wise step size of 8-bit weight quantization, we need  $C + C/r$  real-valued parameters and multiplications for each SE-like module. As 4-bit activation quantization uses the layer-wise step size, its parameter cost is negligible. Also, each process of dividing by step size and multiplying by step size can be merged to the preceding normalization and following  $\times \beta$ , respectively.

## D INSTA-Th for different block structure

In recent studies [2,21], a different convolution block layer order from the one used in the Bi-real-net [19] has been used. Its layer order is BatchNorm (BN)-Sign-conv-PReLU- $\oplus$ , where  $\oplus$  means element-wise addition of residual path and identity shortcut starting just before BN. To verify the versatility of the proposed method, we also tested INSTA-Th to this block structure. One thing to note is that the normalization layer inside the newly added INSTA-Th comes immediately after the BN of the original structure (BN - Normalization - Sign with modified *TH*). In this case, the scale and shift effect of the original BN layer may be inhibited, and the meaning of the added normalization layer is also faded. To handle this, we tried to merge BN and the newly added normalization

**Table 5.** ImageNet top-1 validation accuracy comparison between the BN-sign-conv layer ordered network with and without INSTA-Th module. When INSTA-Th module is used, its normalization layer replaces a BN layer of the network.

	Top-1 Acc. (%)
BN - sign - binary conv - PReLU	59.5
BN (w/o $\gamma, \beta$ ) - sign - binary conv - PReLU	59.0
INSTA-Th - binary conv - PReLU	60.5

layer (replacing the original BN with the proposed INSTA-Th), and its result is in Table 5. Removing the scale and shift from the original BN brought a slight decrease in accuracy (row 1 and 2), but merging BN and normalization layer of INSTA-Th shows the improved threshold controlling ability (row 1 and 3). This suggests that the proposed INSTA-Th plays a similar role to the shift of BN, but it works instance-wise and improves the performance further. This result supports the effectiveness of the proposed INSTA-Th in various block structures.